LANGMUIR

pubs.acs.org/Langmuir Article

# Formation and Characterization of a Stable Monolayer of Active Acetylcholinesterase on Planar Gold

Joshua M. Correira and Lauren J. Webb*

Cite This: https://doi.org/10.1021/acs.langmuir.1c03399 Read Online

ACCESS | Metrics & More | Article Recommendations

**ABSTRACT:** Enzyme activity is the basis for many biosensors where a catalytic event is used to detect the presence and amount of a biomolecule of interest. To create a practical point-of-care biosensor, these enzymes need to be removed from their native cellular environments and immobilized on an abiological surface to rapidly transduce a biochemical signal into an interpretable readout. This immobilization often leads to loss of activity due to unfolded, aggregated, or improperly oriented enzymes when compared to the native state. In this work, we characterize the formation and surface packing density of a stable monolayer of acetylcholinesterase (AChE) immobilized on a planar gold surface and quantify the extent of activity loss following immobilization. Using spectroscopic ellipsometry, we determined that the surface concentration of AChE on a saturated Au surface in a buffered solution was 2.77 ± 0.21 pmol cm$^{-2}$. By calculating the molecular volume of hydrated AChE, corresponding to a sphere of 6.19 nm diameter, divided by the total volume at the AChE−Au interface, we obtain a surface packing density of 33.4 ± 2.5% by volume. This corresponds to 45.1 ± 3.4% of the theoretical maximum monolayer coverage, assuming hexagonal packing. The true value, however, may be larger due to unfolding of enzymes to occupy a larger volume. The enzyme activity and kinetic measurements showed a 90.6 ± 1.4% decrease in specific activity following immobilization. Finally, following storage in a buffered solution for over 100 days at both room temperature and 4 °C, approximately 80% of this enzyme activity was retained. This contrasts with the native aqueous enzyme, which loses approximately 75% of its activity within 1 day and becomes entirely inactive within 6 days.

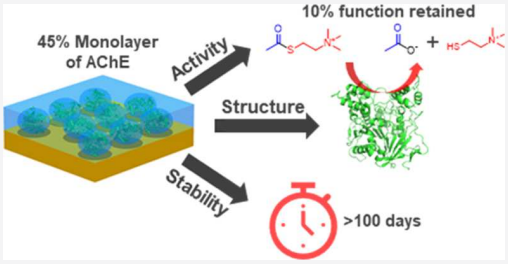




## INTRODUCTION

Enzymes offer attractive capabilities in a wide variety of biosensing and catalysis applications. They are efficient, with catalytic rates up to $10^9$ $M^{-1}$ $s^{-1}$ when limited only by diffusion, often exceptionally specific toward their substrates, and operate under mild conditions in aqueous solution at ambient temperature and pressure.[1,2] However, enzymes suffer from low stability and reusability, which often requires separation of the enzyme from the matrix, when used as catalysts and sensors in aqueous solution.[3,4] It has been demonstrated that these issues can possibly be overcome if the enzyme can be immobilized on a solid surface or substrate, which often appear to have stabilizing effects on enzymes. There are two proposed reasons for this apparent enhancement in stability. (1) Proteins at the surface/water interface exhibit reduced motion, which leads to less inactivation through transient unfolding and aggregation; this is a productive effect. (2) Unstable forms of the enzyme, such as those with intramolecular cleavages from proteolytic enzymes during purification, become immediately inactivated on immobilization; this is an unproductive effect that generates a surface containing a fraction of inactive enzyme molecules.[5−8] However, despite apparent enhancements in stability, it has long been known that enzymes often inactivate upon interacting with surfaces by unfolding and orienting improperly.[9,10] Unfolding alters the secondary, tertiary, and quaternary structures of enzymes that allow them to perform their functions, resulting in decreased activity. Improper orientation hinders access to the enzyme active site by substrate molecules if it is blocked by the surface or by neighboring enzymes in the densely packed layer of immobilized biomolecules. To overcome this, our goal is to prepare surfaces that control the interactions with enzymes in a way that prevents unfolding and promotes optimal orientation; activity losses can then be minimized and the benefits of surface immobilization can be fully realized.

Common methods of enzyme immobilization include adsorption,[11−19] covalent attachment,[20−24] entrapment in porous networks,[13,25−28] and affinity binding.[29] Each method has its own advantages and disadvantages at controlling enzyme−surface interactions, preventing activity loss, and characterization, and there have been many reports on

Received: December 20, 2021
Revised: February 18, 2022

successes with each.[30−32] First, adsorption, where proteins non-covalently interact with a surface, is the simplest and most studied method. The adsorption process starts with the hydration of the adsorbent surface with the aqueous protein solution and the formation of an ordered water layer at the surface−bulk solution interface. Protein molecules then rapidly diffuse into the ordered water layer and displace an equal volume of interfacial water. The energy associated with this dehydration is related to the hydrophilicity of the adsorbent surface; it requires more energy to dehydrate a more hydrophilic surface, which leads to lower levels of protein adsorption.[33] These direct interactions between the proteins and the adsorbent surface are difficult to predict and control. The protein can rearrange its secondary and tertiary structure to allow amino acid side chains to interact favorably with the surface/solvent interface, as well as orient into an energy-minimized configuration where one side of the molecule interacts with the surface and one side interacts with the bulk solution. These rearrangements often result in activity losses as described above. Immobilization by adsorption also often suffers from enzyme leaching, where adsorbed enzyme molecules desorb from the surface over time, leading to additional transient activity losses. Second, covalent attachment strategies attempt to improve this situation by directly binding the enzyme to functional groups displayed on the adsorbent surface, usually through side chains displayed on the enzyme surface, including carboxyl (Asp and Glu), amine (Lys), or thiol (Cys) groups. These covalent bonds prevent enzyme leaching for as long as the bonds remain intact. However, this strategy suffers from lack of site specificity similar to adsorption. Native reactive side chains are often dispersed across the enzyme surface, leading to many possible covalent attachment sites and difficulty in controlling protein orientation. Modifications can be made to the enzyme to introduce reactive groups, both native and nonnative, through mutagenesis or synthetic labeling; however, even slight modifications often come with structural changes that can contribute to activity losses. Third, entrapment strategies attempt to immobilize enzymes by confining them to pores in a material that maintains a native solution-like environment, such as a silica sol−gel, polysaccharide-based gels, or carbon paste. This has the potential to overcome the disadvantages with direct protein−surface interactions involved in adsorption and covalent attachment. However, the confinement of enzymes within porous materials often introduces physical barriers limiting substrate diffusion to the enzyme, reducing sensor activity. Additionally, the enzyme may still be able to directly interact with the porous material leading to activity losses, similar to adsorption and covalent attachment. This strategy can also suffer from enzymes leaching from the porous material, leading to a reduced activity over time. Finally, affinity binding strategies have the potential to overcome the lack of specificity of covalent bonding and adsorption strategies while retaining the strong binding interactions of covalent attachment. Common affinity strategies include biotinylated enzymes binding to surface-bound streptavidin, histidine-tagged enzymes binding to surface-bound nickel ion chelators, and enzymes binding to aptamers generated through directed evolution.[30,34,35] However, these strategies suffer from many of the same disadvantages as adsorption and covalent attachment.

Additional challenges of generating active, stable, useful biosensors and catalysts come from the difficulty of characterizing proteins immobilized on surfaces. The common types of characterization include quantifying the amount, secondary structure, and activity of the immobilized protein. However, studies rarely report all of these important characteristics simultaneously or even under similar conditions, and there is a significant inconsistency across the community about what constitutes an active surface-associated enzyme. The common techniques for determining the amount of immobilized protein include quartz crystal microbalance with dissipation (QCM-D),[11,36] surface plasmon resonance,[37] ellipsometry,[38,39] Fourier transform infrared (FTIR) spectroscopy,[21] and solution depletion.[40] Each technique has advantages explained in the literature, but also disadvantages that can result in erroneous or unrepresentative conclusions when overlooked. For example, QCM-D has frequently been used to determine the mass of adsorbed or immobilized materials by measuring the change in resonant frequency of an oscillating quartz crystal as mass adsorbs, desorbs, or binds. It has also long been known that the determined mass includes that of solvent molecules coupled to the quartz crystal, which largely overestimates the actual mass of adsorbed or immobilized materials. The analysis is complicated further when measuring flexible molecules, such as proteins; the relationship between resonant frequency and mass becomes more difficult to model.[39,41,42] Additionally, the quartz crystal is often used as a proxy of the actual surface of interest, even if the method of immobilization or adsorption is drastically different between the two. Furthermore, immobilization onto quartz crystals usually occurs under laminar flow conditions, often very different from the equilibrium conditions of kinetic measurements. Finally, oscillations of the crystal itself can affect adsorption, making it difficult to separate effects of the measurement itself on the system of interest.[43] QCM-D is not an anomaly in this regard. When spectroscopic techniques such as FTIR and ellipsometry are performed in air, the biomolecular surface is often rinsed in pure water and then dried. This treatment rinses away the salts and ions and dehydrates the protein, all of which can lead to additional structural changes and activity loss. Measurements made on protein-coated samples in air are therefore likely unrepresentative of protein-coated samples stored in a buffered solution, as proteins natively exist. This trend of making measurements, such as the amount of immobilized protein, on a proxy surface under one set of conditions and making additional measurements, such as activity, on a different surface under entirely different conditions, significantly complicates building and studying reliable, robust, and reproducible sensors and catalysts. Additionally, many enzyme-based sensors may unintentionally use impure forms of the enzyme, purchased commercially on a basis of total activity. The total activity depends on the total amount of enzyme of interest present in the sample, and it is often not specified what else is present, for example, salts, detergents, and other proteins. A problem arises when a large composition of the sample is composed of other proteins. When immobilizing the enzyme of interest onto a surface, through common non-specific techniques mentioned above, from a solution that contains an abundance of other proteins, the resulting surface will only contain a fraction of the expected enzyme of interest. This results in lower surface concentrations of the active enzyme than desired. All of these challenges will be addressed in detail here.

In this work, we present the characterization of a stable active monolayer of the enzyme acetylcholinesterase (AChE) adsorbed on bare gold, a model system useful for investigating the properties of an active enzyme immobilized on a surface


https://doi.org/10.1021/acs.langmuir.1c03399
Langmuir XXXX, XXX, XXX−XXX

where interactions to control folding and orientation are not present. Additionally, for the reasons mentioned above, AChE-coated surfaces were measured and prepared under a single set of identical conditions, using purified forms of the enzyme, in which all samples were kept in buffered solutions at all times during all measurements. AChE is a serine hydrolase involved in impulse termination in the central and peripheral nervous systems by hydrolyzing the neurotransmitter acetylcholine at the synapse. It is extremely efficient with a rate constant approaching $10^9$ $M^{-1}$ $s^{-1}$, near the physical catalytic limit controlled by diffusion.[2] AChE is known to be inhibited by various organophosphates and carbamates, such as pesticides and nerve agents; its inhibition results in an accumulation of acetylcholine at the synapse and can be fatal.[44,45] It was chosen as the model enzyme in this study since changes in its high activity following immobilization on Au can be easily observed using a sensitive spectroscopic assay. Additionally, its inhibition can be used as a detection strategy for organophosphate compounds in point-of-use sensors.[44] It is also a desirable candidate for future work relating to orientational control because of its structure-wide dipole moment of approximately 1000 D, which projects through the middle of the active site. The entrance to the active site is at the negative end of the dipole, at the mouth of the so-called "active site gorge" that channels substrates to the active site on the opposite end of the enzyme.[46] Simulations have already shown that immobilization on charged self-assembled monolayers can direct the orientation of AChE based on this dipole.[47] In this work, AChE immobilized on bare Au was characterized by investigating its surface concentration, packing density, structural changes, and activity retention following immobilization and storage with time using spectroscopic ellipsometry (SE) and attenuated total reflectance (ATR) FTIR spectroscopy. We show using SE and ATR that a precise surface concentration can be determined for AChE as it saturates the Au surface. We also show using ATR that the secondary structure of AChE following immobilization is significantly altered from previous reports of aqueous AChE but is largely independent of packing density. The activity retention of AChE following immobilization was investigated using a kinetic spectroscopic assay of acetylcholine hydrolysis. We show there are diffusion limitations that lower the apparent activity of immobilized AChE; upon overcoming these limitations at sufficiently high substrate concentrations, the true activity loss associated with AChE adsorption on Au from other factors becomes apparent. Our aim is that the experiments performed and the results obtained here will serve as the foundation for future work involving the preparation and characterization of enzyme-based sensors and catalysts where the interactions between the enzyme and surface are controlled.

## MATERIALS AND METHODS

**Gold Surface Preparation.** Si(111) wafers (EL-CAT Inc.) were coated with 10 nm of Ti and 100 nm of Au in a PVD75 (Kurt J. Lesker Co.) electron beam deposition chamber at a pressure of less than $5 \times 10^{-6}$ Torr. Wafers were then diced into $10.5 \times 10.5$ $mm^2$ sections using a DAD-321 (Disco) dicing saw. For SE measurements, the wafers were diced into $25.5 \times 10.5$ $mm^2$ sections. Immediately prior to use, the surfaces were gently polished with an optical grade lens tissue (Thorlabs) moistened with high-purity water to remove debris from the dicing process, immersed in piranha solution (3:1 mixture of concentrated $H_2SO_4$ and 30% $H_2O_2$; *caution: explosive in the presence of organic contaminants*) for 1 min, and then annealed under a $H_2$(g) flame for 5 min.

**AChE Purification.** AChE from electric eel (E. electricus) was purchased from MilliporeSigma (catalog C2888, 5000 U, specific activity approximately 600 U $mg^{-1}$) and purified by size exclusion chromatography before use.[48] AChE (5000 U, approx. 6.5 mg total solid) was dissolved in 650 $\mu$L of running buffer (100 mM sodium phosphate, 400 mM NaCl, and pH 7) and injected into a Superdex 200 (Cytiva) size exclusion chromatography column at a flow rate of 0.5 mL $min^{-1}$. AChE was separated and eluted in a single peak and was concentrated using Amicon Ultra 0.5 mL 10K spin filters at 14,000*g*. AChE was exchanged into a 100 mM sodium phosphate pH 7 buffer using a PD-10 desalting column (Cytiva) and stored at −80 °C until use. The specific activity following purification was approximately 5000 U $mg^{-1}$. Purity was confirmed using sodium dodecyl sulfate-polyacrylamide gel electrophoresis (SDS-PAGE).

**AChE Surface Preparation.** AChE-coated surfaces were prepared through direct adsorption. For activity and ATR experiments, 50 $\mu$L of 500 nM AChE (0.035 mg $mL^{-1}$) was placed in contact with a freshly prepared Au surface in a home-built polytetrafluoroethylene (Teflon) liquid cell with a 0.32 $cm^2$ exposed area for 1 h. For SE experiments, 150 $\mu$L of 500 nM AChE was placed in contact with a freshly prepared $25.5 \times 10.5$ $mm^2$ Au surface in a home-built stainless steel liquid cell with a 2 $cm^2$ exposed area for 1 h. This allowed for reproducible amounts of AChE solution contacting the Au and reduced the amount of the sample used. After 1 h, the AChE solution was rinsed away by 3 volumes of 100 mM sodium phosphate pH 7 buffer. The AChE-coated surface was then removed from the liquid cell, placed in a storage vial, and rinsed further by 5 volumes each of 100 mM sodium phosphate pH 7 and pH 8 buffers. The surface was stored overnight at room temperature or 4 °C under pH 8 buffer to fully desorb loosely bound AChE. The purpose of the rinsing process was to leave behind only strongly bound AChE that is directly interacting with the gold and remove weakly bound AChE that can desorb during future experiments. This also results in reproducible responses of the AChE-coated surface as would be expected for a sensor based on this system.

**AChE Activity Assay.** The activity of AChE in solution or immobilized on Au was measured following a spectroscopic assay adapted from Ellman.[49] Briefly, this assay replaced the native substrate acetylcholine with a thioester variant, acetylthiocholine (ATCh), which was hydrolyzed by AChE into thiocholine and acetate. Thiocholine was then labeled by Ellman's reagent, 5,5-dithio-bis-(2-nitrobenzoic acid) (DTNB). The reaction between DTNB and ATCh released 1 equiv of thio-2-nitrobenzoic acid (TNB) anion, which absorbs strongly at 412 nm ($\varepsilon = 1.36 \times 10^4$ $M^{-1}$ $cm^{-1}$) as a measure of the amount of ATCh hydrolyzed over the specific assay time frame. To do this, 3 mL of 100 mM sodium phosphate pH 8 was added to a disposable cuvette or vial. Then, either 10 $\mu$L of AChE solution (10 nM) or 1 AChE-coated Au surface was added to the cuvette or vial, respectively, followed by 20 $\mu$L of DTNB (0.01 M in a buffer composed of 100 mM sodium phosphate pH 7 and 0.018 M $NaHCO_3$) and 20 $\mu$L of 0.075 M ATCh. The reaction was initiated by mixing the cuvette with a pipette or by swirling the vial. For AChE in solution, the reaction was allowed to run for 2 min without stirring and was quenched by adding 100 $\mu$L of 2% sodium dodecyl sulfate and mixing to inactivate AChE. For surface-bound AChE, the reaction was allowed to run for 2 min without stirring and was quenched by removing the liquid from the vial and placing it in a cuvette. Prior to removing the liquid, the vial was swirled to homogenize the TNB anion in solution. Removing the liquid from the vial separates the assay reagents from the surface-bound AChE and stops the reaction. In cases of loosely bound AChE, there can be desorbed protein in solution that allows the reaction to continue in the cuvette following removal of the surface. If this occurred, the surfaces were rinsed and stored overnight under pH 8 buffer before the measurement was repeated. This was only observed for surfaces prepared with AChE concentrations at or above 250 nM, where higher amounts of AChE were present on the surface. Once the reaction was quenched, the absorbance was measured at 412 nm to quantify the amount of ATCh


https://doi.org/10.1021/acs.langmuir.1c03399
Langmuir XXXX, XXX, XXX−XXX

hydrolyzed and determine the initial reaction velocity and specific activity. The specific activity of AChE is reported as 1 U $mg^{-1}$ = 1 $\mu$mol of ATCh hydrolyzed per min per milligram of AChE present.

**Spectroscopic Ellipsometry.** The surface concentration of AChE immobilized on Au stored in a buffered solution was probed using SE. SE experiments were performed using a M-2000 ellipsometer (J.A. Woollam). AChE-coated Au surfaces (25.5 × 10.5 $mm^2$) stored under pH 8 buffer (100 mM sodium phosphate) were placed in a previously aligned liquid cell (J.A. Woollam) mounted onto the ellipsometer stage without rinsing or drying. The liquid cell was then loaded with approximately 500 $\mu$L of pH 8 buffer, and SE data were collected from 190 to 1700 nm at an incident angle of 70° (fixed by the windows on the liquid cell). The liquid cell allowed the AChE-coated Au surface to remain under buffer during measurements while ensuring the light entered the liquid ambient above the surface at a normal incidence. The resulting SE data were analyzed using the CompleteEASE software (J.A. Woollam). Analysis was constrained to 400−1000 nm due to high depolarization of the reflected beam from the liquid cell and Au surface, which resulted in noisy data and a poor fit outside this range.

The AChE-coated gold surface was described by a model consisting of a gold substrate, with optical functions $n(\lambda)$ and $k(\lambda)$ and an infinite thickness, with a transparent protein layer on top, with optical functions $n(\lambda)$ and $k(\lambda)$, and a finite thickness. The optical functions (refractive index, $n$, and extinction coefficient, $k$, as a function of wavelength $\lambda$) of the gold substrate were determined by measuring a bare Au substrate in pH 8 buffer and fitting the data to a B-spline. The optical functions of the transparent protein layer were modeled by a Cauchy dispersion function, as shown in eq 1

$$n(\lambda) = A + \frac{B}{\lambda^2} + \frac{C}{\lambda^4} \quad (1)$$

where $A$, $B$, and $C$ are the fit parameters. The Cauchy dispersion function requires the layer to be transparent and thus $k(\lambda) = 0$. To determine the surface concentration of AChE, both the refractive index and the thickness of the protein layer need to be determined. However, in layers under 10−20 nm thickness, SE is not sensitive to the optical constants and thickness alone but is sensitive to the optical thickness (thickness−index product). Additionally, the refractive index and thickness are inversely correlated in layers under 10−20 nm thickness. This means that the refractive index and thickness cannot be simultaneously determined as there is a range of solutions that adequately fit the data and give the same optical thickness. To overcome this, either refractive index or thickness is often fixed at an assumed value and the other is fit, allowing a unique solution to be obtained at the assumed value.[50] In this case, the thickness of the protein layer was assumed to be 7 nm based on the size of AChE in the crystal structure (PDB: 1C2O),[48] and the Cauchy parameter, $A$, was fit to determine the refractive index. Notably, the absolute value of the determined refractive index may be inaccurate since it relies on the assumed thickness. Despite this, the optical thickness, to which SE is sensitive, remains constant regardless of the assumed thickness due to the inverse correlation between refractive index and thickness. Conveniently, the surface concentration can then be calculated from the optical thickness, which circumvents the insensitivity to refractive index and thickness alone. This is shown below in eq 2

$$\Gamma = \frac{d(n - n_0)}{\mathrm{MW}(\mathrm{d}n/\mathrm{d}c)} \quad (2)$$

where $\Gamma$ is the surface concentration in mol $cm^{-2}$, $n$ is the refractive index of the protein layer at 589.3 nm, $n_0$ is the refractive index of the ambient buffer ($n_0$ = 1.334 at 589.3 nm), $d$ is the fixed thickness of the protein layer in centimeters, $dn/dc$ is the refractive index increment, and MW is the molecular weight of AChE (MW = 69,139 g $mol^{-1}$ for the catalytic unit).[38,39] The thickness−index product in the numerator is the optical thickness. $dn/dc$ describes how the refractive index of the protein layer changes as a function of protein concentration and was calculated for AChE from its amino acid sequence ($dn/dc$ = 0.195 $cm^3$ $g^{-1}$) but is approximately 0.185 $cm^3$ $g^{-1}$ for most proteins.[51] Using a value of 0.185 $cm^3$ $g^{-1}$ for $dn/dc$ in place of 0.195 $cm^3$ $g^{-1}$ only resulted in a 5% difference in the calculated surface concentration.

**Attenuated Total Reflectance.** ATR spectra were collected to confirm the presence of AChE adsorbed onto Au, investigate its packing density, and investigate the changes in its structure following adsorption. The presence of AChE was indicated by the appearance of two absorption bands, amide I and amide II, which correspond to the carbonyl stretching and N−H bending of the amide backbone of the enzyme, respectively.[52] ATR measurements were performed using a Vertex 70 FTIR spectrometer (Bruker) equipped with a liquid $N_2$-cooled HgCdTe (MCT) detector and a single-reflection Ge ATR accessory with a 65° angle of incidence (Harrick) continuously purged with $N_2$(g). Data acquisition and spectral processing were performed using the OPUS software package (Bruker). AChE-coated gold surfaces stored under pH 8 buffer (100 mM sodium phosphate) were removed and then inverted onto the ATR crystal without rinsing or drying to ensure that the buffered solution environment was maintained. Scans were accumulated for 10 min at 4 $cm^{-1}$ resolution, 20 kHz scanner velocity, and a sample signal gain of 2×. Longer scans resulted in the gold surface drying out by evaporation of buffer. Single-channel spectra were first background-corrected using a reference spectrum of the blank Ge ATR crystal and then converted to absorbance spectra. Since the bending mode of liquid water in the buffer strongly overlaps with the amide I absorption of AChE, the corrected spectra were background-corrected again interactively, using a reference spectrum of a blank gold surface in buffer, until the baseline region above 1700 $cm^{-1}$ was flat, indicating adequate water subtraction.[53,54] This treatment was sufficient for most experiments. However, for secondary structure determination, which relies heavily on the line shape of the amide I band, the samples were stored overnight at 4 °C in deuterated buffer (100 mM sodium phosphate, pD = 8) to shift the bending mode away from amide I.[52,55] Absorptions due to residual water vapor in the ATR accessory also overlap with the amide I and II absorptions of AChE and were subtracted interactively using a reference spectrum of moist air. Baseline corrections were performed using a rubber band algorithm.

## RESULTS AND DISCUSSION

**AChE Purification.** First, the purity of commercially purchased AChE was checked by SDS-PAGE, and it was determined to be around 10% pure (data not shown). This is unsurprising since no claims about purity were made from the manufacturer, and the enzyme was sold on the basis of total activity. The initial specific activity of the enzyme, prior to purification, was approximately 600 U $mg^{-1}$. During size exclusion chromatography, approximately 12 peaks were observed, of which the one corresponding to AChE was the largest. The size of the AChE peak is consistent with the purity estimated from SDS-PAGE. Following size exclusion chromatography, the specific activity was approximately 5000 U $mg^{-1}$, indicating a near 10-fold increase in purity. This becomes important during surface immobilization when as much space as possible needs to be occupied by active forms of the enzyme of interest, not other enzymes, as will be discussed in detail later. Thus, it is recommended that purity is confirmed prior to enzyme immobilization for any system.

**AChE Surface Concentration and Structure.** Next, the absolute surface concentration ($\Gamma$) and packing density of AChE on bare Au surfaces were determined by SE. This was done to quantify the total amount of tightly bound AChE adsorbed and determine the specific activity of AChE per unit mass adsorbed to understand what fraction of immobilized AChE is functional (discussed below). Importantly, this was done following the desorption of loosely bound AChE, as will be discussed in detail below. As mentioned above, when fitting


https://doi.org/10.1021/acs.langmuir.1c03399
Langmuir XXXX, XXX, XXX−XXX

the SE data to the model described above in the CompleteEASE software, the thickness of the AChE layer on Au was assumed to be 7 nm based on an estimate of the largest diameter of the AChE catalytic unit in the crystal structure (PDB: 1C2O).[48] This allowed the software to reach a unique solution for $n(\lambda)$ of the AChE layer. However, the absolute value of $n$ is only accurate if the true thickness of the layer is 7 nm. Since the layer thickness was approximated from the crystal structure and assumes that AChE is perfectly spherical, the absolute value of $n$ was likely inaccurate. Regardless, as described above, an absolute value for $\Gamma$ can be determined because the calculation is dependent on optical thickness and results in similar values of $\Gamma$ independent of the assumed layer thickness. Thus, the calculated $\Gamma$ of AChE adsorbed onto bare Au from a bulk solution of 500 nM AChE was determined to be 2.77 ± 0.21 pmol cm$^{-2}$.

Next, to determine what fraction of the surface was occupied by protein, the size of the AChE molecule and the thickness of the protein layer must be accurately known. Notably, since the true value of these parameters could not be determined using the techniques in this work, they must be estimated based on several assumptions. First, the size of AChE was estimated by calculating the protein partial specific volume as the weighted average of the partial specific volumes of each amino acid in its sequence plus an assumed hydration layer of 0.35 mL g$^{-1}$. This estimate is based on an average level of hydration for proteins, which can vary between 0.14 and 1.04 mL g$^{-1}$, and is likely a source of error for this calculation.[51,56] Using these estimates, the hydrated protein partial specific volume was calculated to be 1.08 mL g$^{-1}$, corresponding to a sphere of 6.19 nm diameter representing the volume occupied by the hydrated protein. This agrees approximately with the size of AChE in the crystal structure. Excluding the 0.35 mL g$^{-1}$ hydration water, we calculate a protein partial specific volume of 0.73 mL g$^{-1}$, corresponding to a 5.43 nm diameter sphere representing the volume occupied by the core non-hydrated protein. The difference between the hydrated protein and core protein represents the calculated hydration shell, which corresponds to a 3.4 Å layer, or 2−3 hydration shells, of water. This calculation is consistent with the results we have published previously on the hydration of a surface-bound peptide.[57] These spherical representations of hydrated and core AChE are for convenience only since AChE adopts an ellipsoidal shape. Modeling of an ellipsoidal shape would require AChE to adopt a single orientation on the surface, which is likely not the case as will be discussed below. However, the estimate of partial specific volume is independent of shape and represents the volume occupied by the polypeptide chain of AChE. Thus, by treating the protein layer as a 6.19 nm thick film, constrained by the diameter of hydrated AChE and containing 2.77 pmol cm$^{-2}$ AChE, we determined that 33.4 ± 2.5% of the film by volume is occupied by protein. Following hexagonal packing principles, the film can at most be 74% occupied by the protein. Thus, the measured volume occupied by the protein corresponds to 45.1 ± 3.4% of a maximally packed monolayer of AChE. A scale model of this dimensional analysis is shown in Figure 1. Importantly, this calculation of protein volume and packing density is based on the assumed volume occupied by the amino acid chain, which is independent of the secondary and tertiary structure of AChE. This is considered the smallest possible volume AChE can occupy when the amino acids are efficiently organized in the folded state. Changes in folding may lead to less efficient organization of the

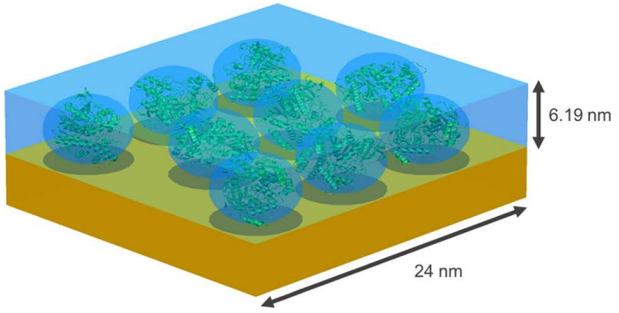


**Figure 1.** Three-dimensional scale model showing 33.4% by volume packing density of AChE on Au corresponding to 45.1% of a maximally packed monolayer based on SE measurements. The green chains show randomly oriented folded AChE enzymes and the blue spheres show a hydrated volume of 6.19 nm diameter. The yellow slab represents the gold surface, and the blue box represents the thickness of the protein layer.

amino acids in the chain and an increase in the volume occupied by AChE, as will be discussed in detail below. Additionally, if a random sequential adsorption model is adopted, then the theoretical maximum packing density would be lower due to the surface exclusion by the existing adsorbed protein molecules and the monolayer fraction would be higher.[58,59] Thus, this calculation of packing density and monolayer fraction is only an estimate based on the measured surface concentration and the several assumptions mentioned here.

Next, to determine the maximum packing density achievable under these conditions, AChE was adsorbed onto bare Au from bulk concentrations ranging from 50 nM to 2 $\mu$M and ATR spectra were collected. A representative spectrum of AChE adsorbed from 500 nM bulk solution is shown in Figure 2a. The amide II band, corresponding largely to the N−H bending mode of the amide backbone of the enzyme,[52] was isolated and fit to a single Gaussian. The intensity of this band is a measure of the amount of adsorbed AChE (Figure 2b).[21,60] The average intensity of each Gaussian is shown plotted against the bulk solution concentration and fit to a Langmuir isotherm in Figure 2c. This shows that the Au surface became saturated with AChE following adsorption when exposed to bulk AChE concentrations above 250 nM. The dashed line shows the theoretical Langmuir isotherm according to eq 3

$$\Gamma = \frac{\Gamma_m C}{C + K_{eq}^{-1}} \tag{3}$$

where $\Gamma$ is the equilibrium surface concentration, $\Gamma_m$ is the theoretical maximum surface concentration, $K_{eq}$ is the Langmuir equilibrium constant, and $C$ is the equilibrium bulk AChE concentration. The amide II intensity was used as a relative measure of surface concentration, and thus, $\Gamma$ and $\Gamma_m$ have units of mAU. $\Gamma_m$ was approximately equal to 1 mAU. The fit was used only as a guide for the eye and no meaningful information was extracted from the fit. This is because in all experiments, the surfaces were rinsed to desorb loosely bound AChE before the measurement.

Rinsing is an important point of debate in the surface science and sensing community.[33] Rinsing is controversial because it disrupts the equilibrium of the system by replacing the bulk enzyme-containing solution with fresh buffer. This means that surface-bound enzymes are no longer in equilibrium with the bulk solution, as is required to assume


https://doi.org/10.1021/acs.langmuir.1c03399
Langmuir XXXX, XXX, XXX−XXX

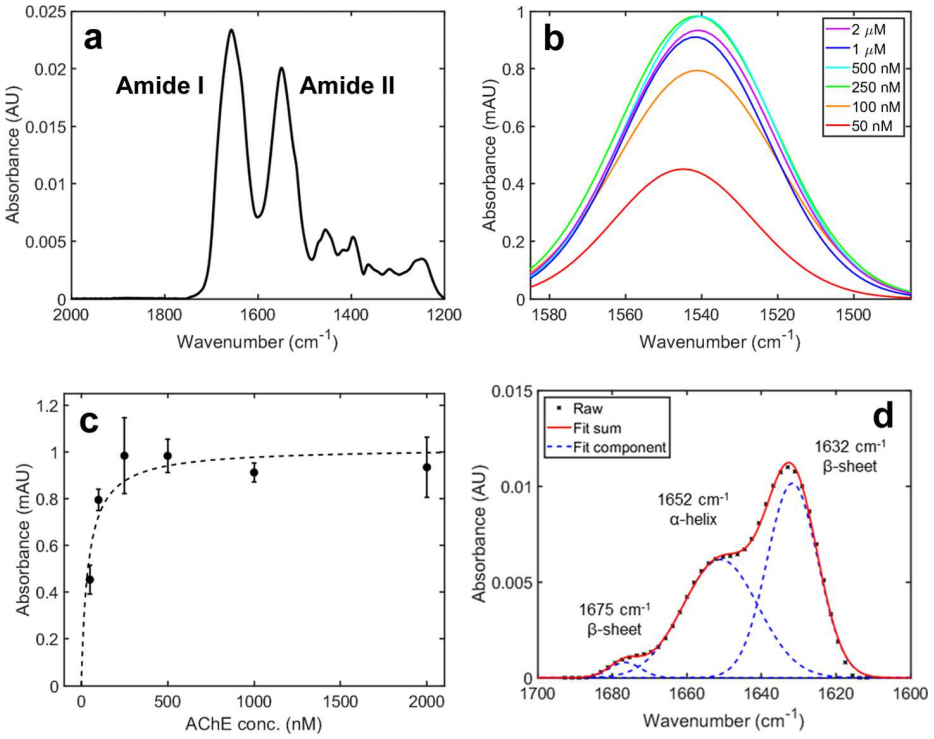


**Figure 2.** (a) Representative ATR spectrum of AChE adsorbed onto bare gold in buffer showing characteristic amide bands (I/II) centered at 1654 and 1548 $cm^{-1}$, respectively. (b) Fit amide II band of AChE adsorbed onto gold from 50 nM, 100 nM, 250 nM, 500 nM, 1 $\mu$M, and 2 $\mu$M bulk concentrations. Each curve is the average of three replicate samples. (c) Plot of average amide II band intensity from (b) as a function of bulk AChE concentration. Error bars indicate the standard deviation of three replicate samples. The dashed line shows the Langmuir isotherm fit (eq 3). (d) Representative band-narrowed amide I band collected in deuterated buffer showing fit to three Gaussian components.

a Langmuir isotherm model. For this reason, the isotherm in Figure 2c was used solely as a guide for the eye. More extensive characterization of the immobilization process can be performed at equilibrium prior to removal of loosely bound protein.[33,61] However, rinsing is an important step to consider, especially in the case of enzymes not covalently bound to surfaces where the attachment may be weaker. In the case presented here of AChE adsorbed on gold, rinsing was necessary to ensure that the results were consistent and stable across all measurements, as would be expected for a useful sensor based on this system. For example, when measuring the activity of immobilized AChE on a poorly rinsed surface, the presence of loosely bound AChE was immediately apparent; AChE loosely bound to the surface appeared to desorb when agitated during the activity assay, which was necessary to homogenize the solution prior to measurement. This resulted in a spike in measured activity compared to what was expected based on well-rinsed surfaces because of desorbed AChE exhibiting a higher level of activity than immobilized AChE, as will be discussed later. Additionally, desorbed AChE remained active in solution even after the assay was quenched by removing the AChE-coated surface. This allowed the assay to continue and the absorbance measured at 412 nm to continuously increase rapidly. The rate of increase of the measured absorbance after quenching is an indication of the amount of desorbed AChE. At most, the rate of increase indicated an amount of desorbed AChE roughly equal to 10% of the total amount of immobilized AChE present. This will be discussed in more detail later. Due to the spike in activity, these results were discarded since it was difficult to deconvolute the activity of immobilized AChE from AChE that desorbed during the assay. Thus, to accurately measure the activity of immobilized AChE, the surfaces were rinsed until only tightly bound AChE remained. This often meant storing overnight in buffered solutions and repeating the activity assay until consistent measurements were achieved. These results suggest that eventually a stable tightly bound layer of AChE remained on the surface. In the case of sensors, responses are often based on the enzyme activity, and thus, the removal of loosely bound enzymes may be required to ensure consistent responses, at the expense of more extensive characterization at equilibrium. Additionally, when performing a measurement with a sensor, the system must be taken out of its original environment, in which it may have established equilibrium, and placed into a sensing environment to detect an analyte of interest. The loosely bound protein can rapidly desorb and interfere with the measurement. Thus, in many cases, rinsing is recommended until consistent measurements can be achieved.

Lastly, to investigate the secondary structure of immobilized AChE, ATR spectra were collected under saturating conditions from a bulk solution concentration of 500 nM. The spectra were collected in both $H_2O$ and deuterated buffer. A representative spectrum, collected in $H_2O$ buffer, is shown in Figure 2a. The amide I band, corresponding largely to the carbonyl stretching of the amide backbone, was isolated, band-narrowed by second derivative analysis, and fit to a sum of three Gaussian components.[55,62] A representative fit is shown in Figure 2d for immobilized AChE in deuterated buffer. The absorption frequency of amide I has been shown to be highly dependent on the secondary structure of enzymes, varying between 1700 and 1600 $cm^{-1}$. Fitting the band-narrowed


https://doi.org/10.1021/acs.langmuir.1c03399
Langmuir XXXX, XXX, XXX−XXX

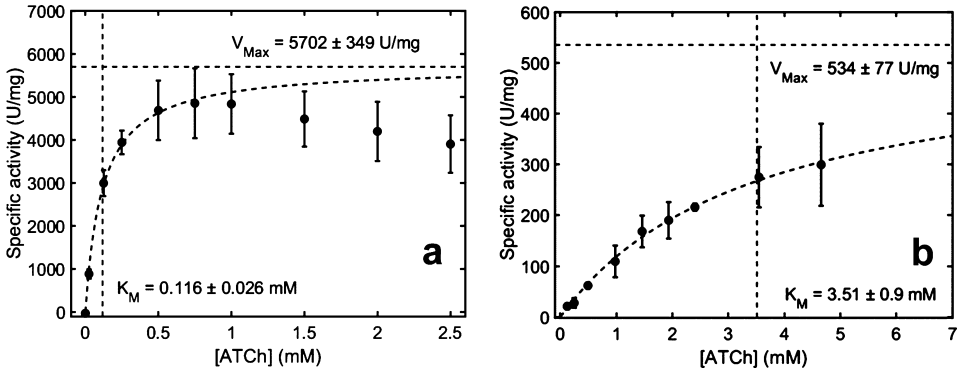


**Figure 3.** (a) Michaelis–Menten kinetics of AChE in solution and (b) adsorbed on bare gold. Substrate inhibition occurs in solution at ATCh concentrations above 1 mM. Error bars indicate a standard deviation of at least three measurements. Dashed lines show fits to the Michaelis–Menten equation (eq 4).

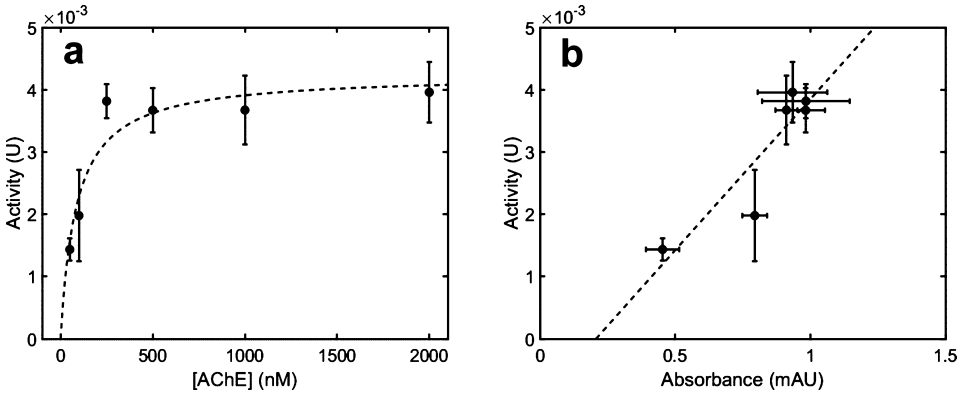


**Figure 4.** (a) Activity of AChE adsorbed onto gold from 50 nM, 100 nM, 250 nM, 500 nM, 1 $\mu$M, and 2 $\mu$M bulk concentrations. The dashed line shows a fit to a Langmuir isotherm (eq 3). (b) Activity from (a) vs corresponding absorbance from Figure 2b. Horizontal and vertical error bars indicate a standard deviation of three replicate samples. The dashed line shows a linear fit to guide the eye.

amide I band to a sum of Gaussian components allows the individual contributions of each type of secondary structure to be determined based on the frequency and area under each component.[52] This was done for AChE immobilized on bare gold, and it was determined that AChE exhibits the characteristics of a 60 ± 2% $\beta$-sheet, a 38 ± 2% $\alpha$-helix, and a 2 ± 4% $\beta$-turn in deuterated buffer. This differs from previous reports of native AChE in solution and calculations based on the crystal structure, where the characteristics of approximately 30% less $\beta$-sheet, 15% more $\beta$-turn, and 15% irregularity were identified. This suggests that AChE unfolds or alters its structure upon immobilization.[63] However, notably, no disordered structure was determined as a result of the fitting. This is due to the limitations of this technique and will be discussed below.

**AChE Activity Retention.** The activity of AChE was measured using a spectroscopic assay to compare the kinetics of immobilized AChE to the kinetics of native aqueous AChE and understand what fraction of immobilized AChE is functional. Michaelis–Menten kinetics were analyzed for AChE in aqueous solution (Figure 3a) and immobilized on bare gold (Figure 3b) by measuring the specific activity as a function of bulk ATCh concentration to investigate the mass transport and kinetic effects on activity. In both cases, the shape of the resulting curve was linear at low ATCh concentrations, relating to the rate of mass transport to the AChE active site, before saturating at high ATCh concentrations, where the rate of mass transport exceeds the catalytic rate and the reaction becomes kinetically controlled.[64] In the case of aqueous AChE, saturation occurred around 1 mM ATCh. Michaelis–Menten kinetics were followed below this concentration. Above this, substrate inhibition by ATCh occurred and activity dropped as the ATCh concentration increased further.[65,66] Data in Figure 3 were fit to the Michaelis–Menten model, eq 4

$$v = \frac{V_{\mathrm{Max}}[\mathrm{S}]}{K_{\mathrm{M}} + [\mathrm{S}]} \tag{4}$$

where $v$ is the initial rate of reaction, [S] is the substrate concentration, $V_{\mathrm{Max}}$ is the maximum achievable rate at saturation, and $K_{\mathrm{M}}$ is the Michaelis constant, equal to [S] at $1/2V_{\mathrm{Max}}$.[67] Here, $V_{\mathrm{Max}}$ is reported in units of specific activity, U mg$^{-1}$. The fit was only determined at ATCh concentrations below 1 mM due to substrate inhibition. As a result of this, AChE never reached the theoretical $V_{\mathrm{Max}}$. The determined value of $K_{\mathrm{M}}$ for aqueous AChE hydrolysis of ATCh was 0.116 ± 0.026 mM, which agrees with previous reports.[65,68] The determined value of $V_{\mathrm{Max}}$ for aqueous AChE hydrolysis of ATCh was 5702 ± 349 U mg$^{-1}$, which is about half the value obtained in previous reports, likely due to the differences in preparation, purification, and assay conditions.[69,70] In the case of immobilized AChE, saturation was never experimentally achieved, and the reaction was largely mass transport controlled, even at ATCh concentrations of 5 mM. Additionally, $V_{\mathrm{Max}}$ was lower by 90.6 ± 1.4%. We believe that this was


https://doi.org/10.1021/acs.langmuir.1c03399
Langmuir XXXX, XXX, XXX−XXX

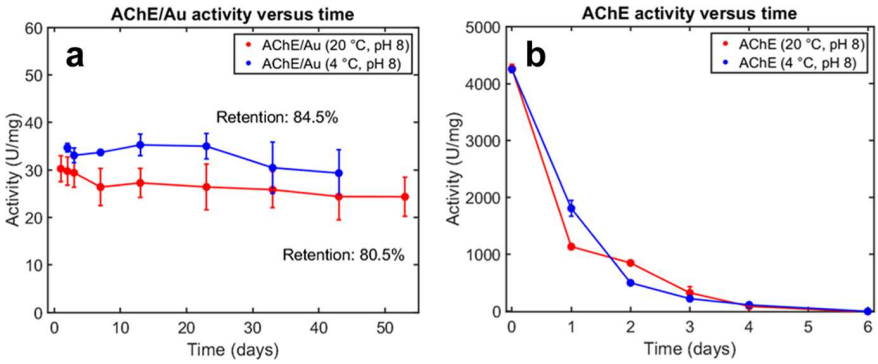


**Figure 5.** (a) Activity retention of AChE immobilized on bare gold and (b) in solution and stored at either 20 °C (red) or 4 °C (blue). ATCh concentrations were 0.5 mM in both cases. The AChE solution concentration was 10 nM. Error bars indicate a standard deviation of three measurements. The same set of samples was measured at each subsequent time point.

due to the effects relating to the immobilization process, such as unfolded or improperly oriented AChE molecules, and explain this below. $K_M$ was higher by a factor of 30 due to the differences between substrate mass transport in bulk and to the planar gold surface, and possibly also owing to a decrease in affinity toward ATCh.[7,64,71]

The activity of AChE adsorbed on bare gold was also investigated as a function of bulk AChE concentration and fit to a Langmuir isotherm, as described above in eq 3 (Figure 4a). This was done to understand if the activity of immobilized AChE is affected by packing density. As shown already in Figure 2b, the average intensity of the amide II band in the ATR spectra, used as a measure of AChE surface concentration, was a function of bulk AChE concentration up to 250 nM. Above this value, the surface saturated and no additional density was observed. In Figure 4, the activity followed the same trend as the amide II intensity: increasing and then saturating at or above a bulk concentration of 250 nM. The measured activity was then related to the surface concentration by plotting against the average amide II intensity from Figure 2; this is shown in Figure 4b. The linear relationship between these two parameters indicates that the activity of immobilized AChE is not affected by packing density and instead increases linearly with the amount of AChE present, as will be discussed below.

Last, the retention of AChE activity immobilized on bare Au (Figure 5a) and in solution (Figure 5b) was investigated by measuring the specific activity over time during storage at room temperature and 4 °C in buffered solution at pH 8. This was done to determine the stability of the response of the AChE-coated surface compared to aqueous AChE with respect to time and repeated use under common storage conditions, important considerations for biological sensors and catalysts. In dilute concentrations under 0.5 $\mu$M AChE, regardless of storage conditions, AChE in solution was observed to lose activity at higher rates than immobilized AChE. Figure 5b shows the complete inactivation of AChE stored at 10 nM in pH 8 buffer at room temperature and 4 °C following 6 days of storage. In contrast, as shown in Figure 5a, immobilized AChE lost only approximately 20% of its activity after over 110 days of storage, the longest we have measured (data only shown for the first 50 days). This stability with respect to time and repeated use appeared to be a function of AChE concentration. When stored in solution at concentrations above 0.5 $\mu$M, AChE exhibited levels of stability similar to immobilized AChE. This is likely due to stabilizing protein−protein interactions present at higher concentrations. The local concentration of AChE on the surface was 4.5 mM (1 pmol confined to a 6.19 nm-thick volume), which may contribute to the observed stability. Additionally, this is only an upper bound on the loss of activity. For reasons described above, the actual activity decrease may have been lower since the first few data points decreased sharply, likely due to desorption of residual loosely bound protein. The response of the AChE-coated surface stabilized after the first few data points were collected, around day 5.

**Discussion.** In this work, our aim was to develop and characterize a model enzyme-based system to learn fundamental principles about making and measuring protein−surface interactions that are relevant to the biosensor and biocatalyst communities. To do this, we prepared and characterized this AChE model system under a single set of conditions that maintained the buffered solution environment around the enzyme at all times. This allowed us to compare all the results obtained through a variety of different measurements directly without making assumptions or approximations that are required when different aspects of structure and function are measured under vastly different conditions. We have shown that the structure, surface concentration, and activity of a model enzyme, AChE, immobilized on gold can be precisely measured under identical conditions in buffered solutions. We have used these results to investigate and understand the differences in performance between immobilized and aqueous enzymes in a system relevant to sensing and catalysis. These differences highlight reasons why sensors and catalysts involving immobilized enzymes often exhibit lower levels of activity and poorer performance than their aqueous counterparts. Yet, we have shown that despite decreased activity, the system continues to perform for months beyond the same enzyme in aqueous solution, highlighting a major benefit of enzyme immobilization. If the initial loss of activity associated with immobilization can be overcome, then this can truly be appreciated. We will discuss our findings further as it relates to this idea.

First, AChE was found to saturate a bare Au surface at bulk solution concentrations of 250 nM AChE or higher; after removal of loosely bound protein molecules, the resulting surface concentration was 2.77 ± 0.21 pmol cm$^{-2}$. By taking the molecular size of AChE as a 6.19 nm diameter sphere, the packing density of AChE was found to be 33.4 ± 2.5% by volume. This corresponds to 45.1% of a maximally packed monolayer, determined by dividing the packing density by a


https://doi.org/10.1021/acs.langmuir.1c03399
Langmuir XXXX, XXX, XXX−XXX

theoretical maximum packing density of 74% based on hexagonal packing principles of spheres. Proteins have previously been shown to pack into well-ordered arrays consistent with hexagonal packing models.[40] This surface concentration is consistent with a previous study that covalently immobilized AChE onto a Pt foil.[22] This packing density obtained here, however, appears to be undersaturated at only half the theoretical maximum. Another previous study was able to achieve near-maximum packing densities by covalently immobilizing AChE to Si.[21] There are two possible reasons for this observation: (1) the surface is simply saturating at less than the theoretical maximum and (2) the calculated packing density is underestimating the true packing density of the surface by underestimating the molecular size of AChE. We will consider each of these possibilities individually.

First, previous measurements of proteins packing into well-ordered arrays based on hexagonal or square packing principles were performed at equilibrium without the removal of the loosely bound protein. The experiments presented here are focused on the properties of the stable and tightly bound fraction of immobilized AChE in the context of sensors following the removal of loosely bound AChE. It is possible that the surface was originally saturated at a theoretical maximum of 74% density prior to removal of the loosely bound fraction through rinsing. As described earlier, it was estimated that the packing density decreased by approximately 10% following rinsing. However, in situ SE data collected during AChE adsorption under saturating conditions (data not shown) indicate that the packing density is around 35% prior to rinsing, clearly well below the theoretical maximum of 74%. This is also consistent with the estimation that the surface concentration decreases by approximately 10% following rinsing, giving rise to the final packing density of 33.4 ± 2.5% calculated earlier. Since proteins have previously been shown to pack into well-ordered arrays consistent with hexagonal packing models prior to rising, it is likely that the surface is indeed saturating at the theoretical maximum. The obtained 35% density at saturation prior to rinsing is likely an indication that the calculation of packing density is underestimating the true packing density. This brings us to the second possibility.

The calculated packing density could underestimate the true packing density if the molecular size of AChE was inaccurate. Underestimating the molecular size would lead to an underestimation of the packing density. This would be the case if AChE partially unfolded on the surface and occupies a larger volume than calculated. Additionally, at lower packing densities, AChE may flatten and spread out on the surface, again occupying a larger volume and area on the surface than calculated. With the techniques used here, we cannot directly measure the molecular size of immobilized AChE to determine the volume it is occupying. However, we first can look at the changes in its secondary structure following immobilization that may be indicative of unfolding to occupy a larger volume. As shown in Figure 2d, the ATR spectra collected of AChE immobilized on gold can be used to investigate its secondary structure on the surface. It was found that AChE exhibits the characteristics of a 60 ± 2% $\beta$-sheet, a 38 ± 2% $\alpha$-helix, and a 2 ± 4% $\beta$-turn, which differ compared to the previous reports of native AChE in aqueous solution.[63] This is unsurprising for the adsorption of AChE on a bare gold surface, where the protein−surface interactions are uncontrolled and has been shown to be the case for similar systems.[9,72,73] The secondary structure of enzymes is largely stabilized by the tertiary structure, so significant changes in the secondary structure seen here may be indicative of changes in the overall folding of the protein that allow it to occupy a larger volume on the surface and lead to reduced activity, as will be discussed. However, this technique is limited by the poor resolution of broad amide bands arising from the different types of secondary structure. The amide I band in Figure 2d was fit to 3 Gaussian bands to prevent over fitting and bias, despite the existence of more than three types of secondary structures. Twelve unique bands have been reported previously corresponding to $\beta$-sheet, $\beta$-turn, $\alpha$-helix, $3_{10}$-helix, and disordered structure, though it is impractical to fit all of these.[52] In this case, amide I bands were fit to the fewest number of Gaussians that qualitatively matched the spectrum, and the position of each Gaussian was used to identify the associated secondary structure. Due to the broad nature of the Gaussians, it is likely that they encompass more types of secondary structure than the one associated with their position. Thus, especially when a signal is limited by the amount of protein present on the surface, direct quantification is difficult, and this technique is best used to estimate the relative changes in structure following immobilization.

Next, we can look at the changes in the structure of AChE over a range of packing densities to determine if it is spreading to occupy a larger volume at lower packing densities. Proteins have been shown to flatten and spread on sub-saturated surfaces in order to increase protein−surface interactions; this can lead to additional unfolding and activity loss.[7,74] We demonstrated that activity was a linear function of AChE surface concentration, shown in Figure 4b. This indicates that the specific activity of AChE (activity per unit mass of AChE) is constant and not affected by packing density. This suggests that either AChE is not spreading and unfolding to a large extent on sub-saturated surfaces or that these effects are not major contributors to activity loss. The active site is buried within the core of the catalytic unit, so it is possible that these effects are not disruptive to its structure. Additionally, this also suggests that denaturing protein−protein interactions on the surface are not present at higher packing densities, and crowding is not limiting substrate diffusion to the active site. To determine whether additional spreading or unfolding is occurring at lower packing densities, ATR spectra were collected for AChE immobilized on bare gold from bulk concentrations ranging from 50 nM to 2 $\mu$M. As shown in Figure 2, AChE adsorbed from bulk concentrations below 250 nM forms a sub-saturated monolayer. In these same spectra, the amide I band was isolated, normalized, and fit to two Gaussian components (Figure 6), as discussed above. Here, only two Gaussian components were used due to the lower signal achieved at lower packing densities. In Figure 6, it can be seen qualitatively that the overall absorption amide I band did not change significantly as a function of AChE surface concentration. However, the two fit peaks, at 1670 and 1638 $cm^{-1}$, did change systematically. The peak centered at 1670 $cm^{-1}$ is indicative of the $\beta$-turn characteristic and increased in relative amount as the AChE surface concentration decreased. The fit component centered at 1638 $cm^{-1}$ is indicative of the $\beta$-sheet characteristic and decreases in relative amount as the AChE surface concentration decreases. This indicates that there are minor, but systematic, losses of ordered structure with decreasing AChE packing density. Additionally, these minor structural changes did not affect the specific activity and thus likely do not disrupt the active site buried in the enzyme.


https://doi.org/10.1021/acs.langmuir.1c03399
Langmuir XXXX, XXX, XXX−XXX

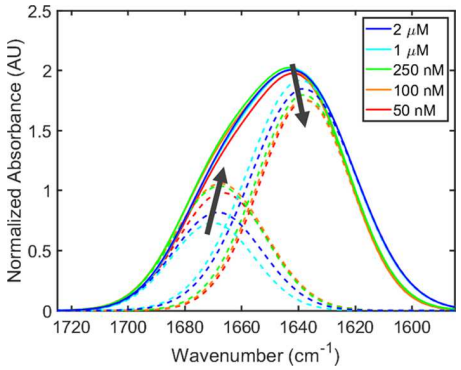


**Figure 6.** Normalized average amide I bands of AChE adsorbed on bare gold from 50 nM, 100 nM, 250 nM, 1 $\mu$M, and 2 $\mu$M bulk concentrations. Each curve represents the average of three measurements. Dashed lines show individual fit components. Solid lines show a sum of fit components to raw data. Arrows show direction of decreasing surface concentration.

Since there are only minor structural changes, the molecular size of AChE is likely not changing much due to spreading over the range of packing densities investigated here. Despite this, because AChE has significantly altered the secondary structure when immobilized on gold, it is likely that it is unfolding to occupy a larger volume than previously calculated. To saturate at a theoretical maximum of 74%, AChE would need to unfold to occupy a volume 2.2 times larger. This corresponds to an approximate 30% increase in diameter. This degree of unfolding is consistent with the high degree of activity loss observed, as will be discussed later. Thus, the most likely possibility is that the surface saturates around the theoretical maximum, with approximately 10% density lost to desorption, but is occupied by AChE that has at least partially unfolded to occupy a larger volume than initially calculated.

These findings highlight the importance of controlling enzyme−surface interactions to prevent unfolding. If AChE could retain its native structure following immobilization, then it would occupy a smaller volume than if it is unfolded, leaving more room for additional enzymes to immobilize. Additionally, retention of the native structure would prevent the high degree of activity loss observed here associated with unfolding, as will be discussed later. The effect of this retention of native structure is a surface containing a greater number of more highly active enzymes. This is especially important in the context of sensors where the loosely bound enzymes must be removed to generate a reproducible sensor response, leaving behind fewer enzymes. In this case, approximately 10% of adsorbed AChE appeared to be loosely bound and readily desorbed during future experiments and rinsing steps. This suggests that there may be preferential adsorption sites on the surface or orientations of AChE that favor tighter surface binding interactions. This will vary depending on surface chemistry and morphology but can further reduce enzyme loading. Thus, clearly, retaining enzyme activity following immobilization is essential.

Next, it was found that AChE lost 90.6 ± 1.4% of its specific activity following adsorption on bare gold but retained over 80% of this remaining activity following storage at room temperature and 4 °C under buffered solutions for over 100 days. In contrast, AChE stored in solution at concentrations under 0.5 $\mu$M lost activity rapidly and became completely inactive within 6 days, as shown in Figure 5. This immediate loss followed by long-term retention of activity of the immobilized enzyme is consistent with the observation that immobilization stabilizes enzymes.[7] This long-term stability may be in part due to surface cysteine residues on AChE that could form gold−sulfur bonds and anchor it to the surface and prevent desorption. The activity of immobilized AChE is lower than the previous reports of AChE covalently bound to modified Pt foil, glass, and Si, likely owing to the direct interactions with a bare and unmodified gold surface.[21,22] This immediate and greater loss of activity of immobilized AChE compared to previous reports is likely due to a combination of surface-induced unfolding, as mentioned earlier, and improperly oriented AChE molecules inhibiting substrate access to the active site. First, for surface-induced folding to result in activity loss, the structure of the active site, and gorge leading to it, may be disrupted. The active site gorge contributes to the high catalytic efficiency of AChE by channeling the substrate and product molecules to and from the surface of the enzyme and the buried active site. Additionally, a breathing motion of the gorge has been shown to be important to this high efficiency.[75] Disruption to the structure of the gorge and hindrance of gorge motion following surface immobilization may contribute to surface-induced activity losses by reducing the substrate and product channeling to and from the active site and making it less available. It is possible that these dynamics may be hindered in the case of tightly bound AChE on the surface, where mobility may be limited. Second, improperly oriented AChE molecules likely account for approximately 10−20% of the observed activity loss. This is based on the relative portion of the surface of the AChE catalytic unit that makes up the entrance to the active site gorge. Assuming a random distribution of orientations on the surface, the entrance to the active site would only be blocked in 10−20% of molecules. Thus, the activity loss observed here is likely dominated by the initial surface-induced unfolding on immobilization. This again highlights the need to control the surface chemistry and protein−surface interactions in a way that prevents surface-induced unfolding and resulting activity losses. As mentioned above, previous reports using modified surfaces observed greater levels of activity following immobilization.

Diffusion limitations can also cause an apparent decrease in specific activity. This is due to the difference in the mass transport rates of substrates and products in bulk versus on a surface. This makes the rate of reaction appear slower when it may simply be limited by a slower rate of mass transport. Michaelis−Menten kinetics highlights these diffusion limitations, with a measured $K_M$ on the surface that was larger than that of solution by a factor of 30. This is due to an effective lower substrate concentration at the surface−solution interface as AChE hydrolyzes substrate faster than it can diffuse to the active site. This requires a higher bulk substrate concentration to achieve the same level of activity as in solution. Interestingly, the $K_M$ obtained here is 1−2 orders of magnitude higher than previous reports of immobilized AChE, which reported $K_M$ values similar to that of aqueous AChE despite being immobilized on a surface.[13,76] It is possible that the additional increase in $K_M$ observed here compared to previous reports is due to a decrease in affinity for ATCh caused by structural changes on the surface, such as disruption to the active site gorge that channels ATCh to the active site or improper orientation of the active site away from bulk solution. Regardless of $K_M$, in the absence of any other effects contributing to activity loss, eventually at high enough


https://doi.org/10.1021/acs.langmuir.1c03399
Langmuir XXXX, XXX, XXX−XXX

substrate concentrations, AChE will achieve the same rate as in bulk solution, free of diffusion limitations.[64,71] However, the observed $V_{Max}$ of AChE immobilized on bare gold is 90.6 ± 1.4% lower than in bulk solution, indicating that there are other effects contributing to activity loss such as surface-induced unfolding and improperly oriented AChE molecules. The level of activity loss is lower than previous reports and suggests a higher degree of unfolding, likely owing to the direct interactions with unmodified gold. There is thus a great motivation to prevent these effects by controlling surface chemistry and protein−surface interactions through chemical modifications of the substrate surface in order to achieve higher levels of packing and activity. Additionally, higher levels of activity bring lower limits of detection for sensors and require lower substrate concentrations. We are currently investigating these possibilities through the techniques employed here.

## CONCLUSIONS

In this work, we have thoroughly characterized the packing density and activity of the enzyme AChE immobilized on bare gold as a model system. We have determined a precise surface concentration for AChE immobilized on gold at saturation using SE and used this value to determine the extent of activity loss following immobilization. The surface concentration and packing density were calculated to be 2.77 ± 0.21 pmol $cm^{-2}$ and 33.4 ± 2.5%, respectively, which corresponds to 45.1 ± 3.4% of a maximally packed monolayer. Accounting for diffusion limitations, we determined a 90.6 ± 1.4% reduction in activity, that is, only ∼10% of surface-bound AChE is operating at the same level as in bulk solution. Based on the packing density and structure of AChE, we estimate that 10−20% of this loss of activity is due to the improperly oriented AChE molecules and the remainder is due to surface-induced unfolding and hindrance of AChE dynamics, highlighting the importance of controlling surface chemistry and protein−surface interactions. This loss of activity was also independent of packing density and only minor, but systematic, structural changes were observed between saturated and sub-saturated packing densities, indicating no additional major unfolding occurred below saturation. This indicates that to achieve a maximum output from a surface-bound enzyme, maximizing enzyme loading, in this case, is preferred since there are no detrimental effects. Additionally, maintaining the native structure can prevent the enzymes from occupying larger volumes and further improve enzyme loading. This work will guide future experiments in our laboratory in the development and characterization of biosensors and biocatalysts based on modified surfaces where protein−surface interactions are controlled.

## AUTHOR INFORMATION


### Corresponding Author

**Lauren J. Webb** − *Department of Chemistry, Texas Materials Institute, and Interdisciplinary Life Sciences Program, The University of Texas at Austin, Austin, Texas 78712-1224, United States;* orcid.org/0000-0001-9999-5500; Email: lwebb@cm.utexas.edu

### Author

**Joshua M. Correira** − *Department of Chemistry, Texas Materials Institute, and Interdisciplinary Life Sciences Program, The University of Texas at Austin, Austin, Texas 78712-1224, United States;* orcid.org/0000-0002-2971-4619

Complete contact information is available at: https://pubs.acs.org/10.1021/acs.langmuir.1c03399


### Notes

The authors declare no competing financial interest.

## ACKNOWLEDGMENTS

This work was supported by the National Science Foundation (grant no. CHE-1807215). We gratefully acknowledge the use of facilities at the Texas Materials Institute at the University of Texas at Austin and the staff at the J.A. Woollam company for their expertise and assistance.

## REFERENCES


(1) Wolfenden, R.; Snider, M. J. The Depth of Chemical Time and the Power of Enzymes as Catalysts. *Acc. Chem. Res.* **2001**, *34*, 938−945.

(2) Stroppolo, M. E.; Falconi, M.; Caccuri, A. M.; Desideri, A. Superefficient Enzymes. Cell. *Mol. Life Sci.* **2001**, *58*, 1451−1460.

(3) Cracknell, J. A.; Vincent, K. A.; Armstrong, F. A. Enzymes as Working or Inspirational Electrocatalysts for Fuel Cells and Electrolysis. *Chem. Rev.* **2008**, *108*, 2439−2461.

(4) Mateo, C.; Palomo, J. M.; Fernandez-Lorente, G.; Guisan, J. M.; Fernandez-Lafuente, R. Improvement of Enzyme Activity, Stability and Selectivity via Immobilization Techniques. *Enzyme Microb. Technol.* **2007**, *40*, 1451−1463.

(5) Sheldon, R. A.; van Pelt, S. Enzyme Immobilisation in Biocatalysis: Why, What and How. *Chem. Soc. Rev.* **2013**, *42*, 6223−6235.

(6) Klibanov, A. M. Enzyme Stabilization by Immobilization. *Anal. Biochem.* **1988**, *93*, 1−25.

(7) Hoarau, M.; Badieyan, S.; Marsh, E. N. G. Immobilized Enzymes: Understanding Enzyme − Surface Interactions at the Molecular Level. *Org. Biomol. Chem.* **2017**, *15*, 9539−9551.

(8) Knotts, T. A.; Rathore, N.; De Pablo, J. J. An Entropic Perspective of Protein Stability on Surfaces. *Biophys. J.* **2008**, *94*, 4473−4483.

(9) Secundo, F. Conformational Changes of Enzymes upon Immobilisation. *Chem. Soc. Rev.* **2013**, *42*, 6250−6261.

(10) Homaei, A. A.; Sariri, R.; Vianello, F.; Stevanato, R. Enzyme Immobilization: An Update. *J. Chem. Biol.* **2013**, *6*, 185−205.

(11) Fleming, B. D.; Praporski, S.; Bond, A. M.; Martin, L. L. Electrochemical Quartz Crystal Microbalance Study of Azurin Adsorption onto an Alkanethiol Self-Assembled Monolayer on Gold. *Langmuir* **2008**, *24*, 323−327.

(12) Reda, T.; Plugge, C. M.; Abram, N. J.; Hirst, J. Reversible Interconversion of Carbon Dioxide and Formate by an Electroactive Enzyme. *Proc. Natl. Acad. Sci. U.S.A.* **2008**, *105*, 10654−10658.

(13) Shulga, O. V.; Jefferson, K.; Khan, A. R.; D'Souza, V. T.; Liu, J.; Demchenko, A. V.; Stine, K. J. Preparation and Characterization of Porous Gold and Its Application as a Platform for Immobilization of Acetylcholine Esterase. *Chem. Mater.* **2007**, *19*, 3902−3911.

(14) Zhang, Y.; Arugula, M. A.; Kirsch, J. S.; Yang, X.; Olsen, E.; Simonian, A. L. Layer-by-Layer Assembled Carbon Nanotube-Acetylcholinesterase/Biopolymer Renewable Interfaces: SPR and Electrochemical Characterization. *Langmuir* **2015**, *31*, 1462−1468.

(15) Thyparambil, A. A.; Wei, Y.; Latour, R. A. Experimental Characterization of Adsorbed Protein Orientation, Conformation, and Bioactivity. *Biointerphases* **2015**, *10*, 019002.

(16) Warning, L. A.; Zhang, Q.; Baiyasi, R.; Landes, C. F.; Link, S. Nanoscale Surface-Induced Unfolding of Single Fibronectin Is Restricted by Serum Albumin Crowding. *J. Phys. Chem. Lett.* **2020**, *11*, 1170−1177.

(17) Ashur, I.; Schulz, O.; Mcintosh, C. L.; Pinkas, I.; Ros, R.; Jones, A. K. Transparent Gold as a Platform for Adsorbed Protein

Spectroelectrochemistry: Investigation of Cytochrome c and Azurin. *Langmuir* **2012**, *28*, 5861−5871.
(18) Dong, A.; Jones, L. S.; Kerwin, B. A.; Krishnan, S.; Carpenter, J. F. Secondary Structures of Proteins Adsorbed onto Aluminum Hydroxide: Infrared Spectroscopic Analysis of Proteins from Low Solution Concentrations. *Anal. Biochem.* **2006**, *351*, 282−289.
(19) Gruian, C.; Vanea, E.; Simon, S.; Simon, V. FTIR and XPS Studies of Protein Adsorption onto Functionalized Bioactive Glass. *Biochim. Biophys. Acta, Proteins Proteomics* **2012**, *1824*, 873−881.
(20) Milkani, E.; Lambert, C. R.; McGimpsey, W. G. Direct Detection of Acetylcholinesterase Inhibitor Binding with an Enzyme-Based Surface Plasmon Resonance Sensor. *Anal. Biochem.* **2011**, *408*, 212−219.
(21) Khaldi, K.; Sam, S.; Gouget-Laemmel, A. C.; Henry De Villeneuve, C.; Moraillon, A.; Ozanam, F.; Yang, J.; Kermad, A.; Ghellai, N.; Gabouze, N. Active Acetylcholinesterase Immobilization on a Functionalized Silicon Surface. *Langmuir* **2015**, *31*, 8421−8428.
(22) Bhatia, S. K.; Cooney, M. J.; Shriver-Lake, L. C.; Fare, T. L.; Ligler, F. S. Immobilization of Acetylcholinesterase on Solid Surfaces: Chemistry and Activity Studies. *Sens. Actuators, B* **1991**, *3*, 311−317.
(23) Mukherjee, S.; Sengupta, K.; Das, M. R.; Jana, S. S.; Dey, A. Site-Specific Covalent Attachment of Heme Proteins on Self-Assembled Monolayers. *J. Biol. Inorg Chem.* **2012**, *17*, 1009−1023.
(24) Hernández-Cancel, G.; Suazo-Dávila, D.; Medina-Guzmán, J.; Rosado-González, M.; Díaz-Vázquez, L. M.; Griebenow, K. Chemically Glycosylation Improves the Stability of an Amperometric Horseradish Peroxidase Biosensor. *Anal. Chim. Acta* **2015**, *854*, 129−139.
(25) Avnir, D.; Braun, S.; Lev, O.; Ottolenghi, M. Enzymes and Other Proteins Entrapped in Sol-Gel Materials. *Chem. Mater.* **1994**, *6*, 1605−1614.
(26) Li, J.; Tan, S. N.; Ge, H. Silica Sol-Gel Immobilized Amperometric Biosensor for Hydrogen Peroxide. *Anal. Chim. Acta* **1996**, *335*, 137−145.
(27) Dave, B. C.; Dunn, B.; Valentine, J. S.; Zink, J. I. Sol-Gel Encapsulation Methods for Biosensors. *Anal. Chem.* **1994**, *66*, 1120A−1127A.
(28) Du, D.; Chen, S.; Cai, J.; Zhang, A. Immobilization of Acetylcholinesterase on Gold Nanoparticles Embedded in Sol − Gel Film for Amperometric Detection of Organophosphorous Insecticide. *Biosens. Bioelectron.* **2007**, *23*, 130−134.
(29) Chumphukam, O.; Le, T.; Cass, A. High Efficiency Acetylcholinesterase Immobilization on DNA Aptamer Modified Surfaces. *Molecules* **2014**, *19*, 4986−4996.
(30) Sassolas, A.; Blum, L. J.; Leca-Bouvier, B. D. Immobilization Strategies to Develop Enzymatic Biosensors. *Biotechnol. Adv.* **2012**, *30*, 489−511.
(31) Jesionowski, T.; Zdarta, J.; Krajewska, B. Enzyme Immobilization by Adsorption: A Review. *Adsorption* **2014**, *20*, 801−821.
(32) Beaufils, C.; Man, H.-M.; de Poulpiquet, A.; Mazurenko, I.; Lojou, E. From Enzyme Stability to Enzymatic Bioelectrode Stabilization Processes. *Catalysts* **2021**, *11*, 497−541.
(33) Vogler, E. A. Protein Adsorption in Three Dimensions. *Biomaterials* **2012**, *33*, 1201−1237.
(34) Jing, M.; Bowser, M. T. Methods for Measuring Aptamer-Protein Equilibria: A Review. *Anal. Chim. Acta* **2011**, *686*, 9−18.
(35) Labib, M.; Sargent, E. H.; Kelley, S. O. Electrochemical Methods for the Analysis of Clinically Relevant Biomolecules. *Chem. Rev.* **2016**, *116*, 9001−9090.
(36) Phan, H. T. M.; Bartelt-hunt, S.; Rodenhausen, K. B.; Schubert, M.; Bartz, J. C. Investigation of Bovine Serum Albumin (BSA) Attachment onto Self-Assembled Monolayers (SAMs) Using Combinatorial Quartz Crystal Microbalance with Dissipation (QCM-D) and Spectroscopic Ellipsometry (SE). *PLoS One* **2015**, *10*, No. e0141282.
(37) Mrksich, M.; Sigal, G. B.; Whitesides, G. M. Surface Plasmon Resonance Permits In Situ Measurement of Protein Adsorption on Self-Assembled Monolayers of Alkanethiolates on Gold. *Langmuir* **1995**, *11*, 4383−4385.
(38) De Feijter, J. A.; Benjamins, J.; Veer, F. A. Ellipsometry as a Tool to Study the Adsorption Behavior of Synthetic and Biopolymers at the Air-Water Interface. *Biopolymers* **1978**, *17*, 1759−1772.
(39) Höök, F.; Vörös, J.; Rodahl, M.; Kurrat, R.; Böni, P.; Ramsden, J. J.; Textor, M.; Spencer, N. D.; Tengvall, P.; Gold, J.; Kasemo, B. A Comparative Study of Protein Adsorption on Titanium Oxide Surfaces Using in Situ Ellipsometry, Optical Waveguide Lightmode Spectroscopy, and Quartz Crystal Microbalance/Dissipation. *Colloids Surf., B* **2002**, *24*, 155−170.
(40) Kao, P.; Parhi, P.; Krishnan, A.; Noh, H.; Haider, W.; Tadigadapa, S.; Allara, D. L.; Vogler, E. A. Volumetric Interpretation of Protein Adsorption: Interfacial Packing of Protein Adsorbed to Hydrophobic Surfaces from Surface-Saturating Solution Concentrations. *Biomaterials* **2011**, *32*, 969−978.
(41) Höök, F.; Rodahl, M.; Brzezinski, P.; Kasemo, B. Energy Dissipation Kinetics for Protein and Antibody - Antigen Adsorption under Shear Oscillation on a Quartz Crystal Microbalance. *Langmuir* **1998**, *7463*, 729−734.
(42) Höök, F.; Kasemo, B.; Nylander, T.; Fant, C.; Sott, K.; Elwing, H. Variations in Coupled Water, Viscoelastic Properties, and Film Thickness of a Mefp-1 Protein Film during Adsorption and Cross-Linking : A Quartz Crystal Microbalance with Dissipation Monitoring, Ellipsometry, and Surface Plasmon Resonance Study. *Anal. Chem.* **2001**, *73*, 5796−5804.
(43) Lacour, F.; Torresi, R.; Gabrielli, C.; Caprani, A.; Upr, C.; Vi, U. P.; Caprani, A. Comparison of the Quartz-Crystal Microbalance and the Double- Layer Capacitance Methods for Measuring the Kinetics of the Adsorption of Bovine Serum Albumin onto a Gold Electrode. *J. Electrochem. Soc.* **1992**, *139*, 1619−1622.
(44) Vinotha Alex, A.; Mukherjee, A. Review of Recent Developments (2018−2020) on Acetylcholinesterase Inhibition Based Biosensors for Organophosphorus Pesticides Detection. *Microchem. J.* **2021**, *161*, 105779.
(45) Colovic, M. B.; Krstic, D. Z.; Lazarevic-Pasti, T. D.; Bondzic, A. M.; Vasic, V. M. Acetylcholinesterase Inhibitors: Pharmacology and Toxicology. *Curr. Neuropharmacol.* **2013**, *11*, 315−335.
(46) Felder, C. E.; Prilusky, J.; Silman, I.; Sussman, J. L. A Server and Database for Dipole Moments of Proteins. *Nucleic Acids Res.* **2007**, *35*, W512−W521.
(47) Yang, S.; Liu, J.; Zheng, H.; Zhong, J.; Zhou, J. Simulated Revelation of the Adsorption Behaviours of Acetylcholinesterase on Charged Self-Assembled Monolayers. *Nanoscale* **2020**, *12*, 3701−3714.
(48) Bourne, Y.; Grassi, J.; Bougis, P. E.; Marchot, P. Conformational Flexibility of the Acetylcholinesterase Tetramer Suggested by X-Ray Crystallography. *J. Biol. Chem.* **1999**, *274*, 30370−30376.
(49) Ellman, G. L. Tissue Sulfhydryl Groups. *Arch. Biochem. Biophys.* **1959**, *82*, 70−77.
(50) Tompkins, H. G.; Hilfiker, J. N. *Spectroscopic Ellipsometry: Practical Application to Thin Film Characterization*; Momentum Press, 2016.
(51) Zhao, H.; Brown, P. H.; Schuck, P. On the Distribution of Protein Refractive Index Increments. *Biophys. J.* **2011**, *100*, 2309−2317.
(52) Yang, H.; Shouning, Y.; Kong, J.; Dong, A.; Yu, S. Obtaining Information about Protein Secondary Structures in Aqueous Solution Using Fourier Transform IR Spectroscopy. *Nat. Protoc.* **2015**, *21*, 382.
(53) Dousseau, F.; Therrien, M.; Pézolet, M. On the Spectral Subtraction of Water from the FT-IR Spectra of Aqueous Solutions of Proteins. *Appl. Spectrosc.* **1989**, *43*, 538−542.
(54) Powell, J. R.; Wasacz, F. M.; Jakobsen, R. J. Algorithm for the Reproducible Spectral Subtraction of Water From the Ft-Ir Spectra of Proteins in Dilute Solutions and Adsorbed Monolayers. *Appl. Spectrosc.* **1986**, *40*, 339−344.
(55) Susi, H.; Michael Byler, D. Protein Structure by Fourier Transform Infrared Spectroscopy: Second Derivative Spectea. *Biochem. Biophys. Res. Commun.* **1983**, *115*, 391−397.


https://doi.org/10.1021/acs.langmuir.1c03399
*Langmuir* XXXX, XXX, XXX−XXX

(56) Durchschlag, H.; Zipper, P. Comparative Investigations of Biopolymer Hydration by Physicochemical and Modeling Techniques. *Biophys. Chem.* **2001**, *93*, 141.
(57) Fies, W. A.; First, J. T.; Dugger, J. W.; Doucet, M.; Browning, J. F.; Webb, L. J. Quantifying the Extent of Hydration of a Surface-Bound Peptide Using Neutron Reflectometry. *Langmuir* **2019**, *36*, 637−649.
(58) Talbot, J.; Tarjus, G.; Van Tassel, P. R.; Viot, P. From Car Parking to Protein Adsorption: An Overview of Sequential Adsorption Processes, Colloids and Surfaces A: Physicochemical and Engineering Aspects 165. *Colloids Surf., A* **2000**, *165*, 287−324.
(59) Schaaf, P.; Talbot, J. Surface Exclusion Effects in Adsorption Processes. *J. Chem. Phys.* **1989**, *91*, 4401−4409.
(60) Fink, D. J.; Hutson, T. B.; Chittur, K. K.; Gendreau, R. M. Quantitative Surface Studies of Protein Adsorption by Infrared Spectroscopy. II. Quantification of Adsorbed and Bulk Proteins. *Anal. Biochem.* **1987**, *165*, 147−154.
(61) Latour, R. A. The Langmuir Isotherm: A Commonly Applied but Misleading Approach for the Analysis of Protein Adsorption Behavior. *J. Biomed. Mater. Res., Part A* **2015**, *103*, 949−958.
(62) Dong, A.; Huang, P.; Caughey, W. S. Protein Secondary Structures in Water from Second-Derivative Amide I Infrared Spectra. *Biochemistry* **1990**, *29*, 3303−3308.
(63) Gorne-Tschelnokow, U.; Naumann, D.; Weise, C.; Hucho, F. Secondary Structure and Temperature Behaviour of Acetylcholinesterase by Fourier-Transform Infrared Spectroscopy. *Eur. J. Biochem.* **1993**, *213*, 1235−1242.
(64) Horvath, C.; Engasser, J.-M. External and Internal Diffusion in Heterogeneous Enzymes Systems. *Biotechnol. Bioeng.* **1974**, *16*, 909−923.
(65) Niday, E.; Wang, C.-S.; Alaupovic, P. Kinetic Evidence for the Allosteric Substrate Inhibition of Human Erythrocyte Acetylcholinesterase. *Biochim. Biophys. Acta* **1980**, *612*, 67−72.
(66) Shafferman, A.; Velan, B.; Ordentlich, A.; Kronman, C.; Grosfeld, H.; Leitner, M.; Flashner, Y.; Cohen, S.; Barak, D.; Ariel, N. Substrate Inhibition of Acetylcholinesterase: Residues Affecting Signal Transduction from the Surface to the Catalytic Center. *EMBO J.* **1992**, *11*, 3561−3568.
(67) Johnson, K. A.; Goody, R. S. The Original Michaelis Constant: Translation of the 1913 Michaelis-Menten Paper. *Biochemistry* **2011**, *50*, 8264−8269.
(68) Shafai, T.; Cortner, J. A. Human Erythrocyte Acetylcholinesterase I. Resolution of Activity Into Two Components. *Biochim. Biophys. Acta* **1971**, *236*, 612.
(69) Parker, K. K.; Chan, S. L.; Trevor, A. J. Purification of Native Forms of Eel Acetylcholinesterase: Active Site Determination. *Arch. Biochem. Biophys.* **1978**, *187*, 322.
(70) Berman, J. D.; Young, M. Rapid and Complete Purification of Acetylcholinesterases of Electric Eel and Erythrocyte by Affinity Chromatography. *Proc. Natl. Acad. Sci. U.S.A.* **1971**, *68*, 395−398.
(71) Goldstein, L. Kinetic Behavior of Immobilized Enzyme Systems. *Methods Enzymol.* **1976**, *44*, 397−443.
(72) Miklos, A. C.; Li, C.; Sharaf, N. G.; Pielak, G. J. Volume Exclusion and Soft Interaction Effects on Protein Stability under Crowded Conditions. *Biochemistry* **2010**, *49*, 6984−6991.
(73) Norde, W.; Anusiem, A. C. I. Adsorption, Desorption and Re-Adsorption of Proteins on Solid Surfaces. *Colloids Surf.* **1992**, *66*, 73−80.
(74) MacRitchie, F. Spread of Monolayers of Proteins. *Adv. Colloid Interface Sci.* **1986**, *25*, 341−385.
(75) Cheng, S.; Song, W.; Yuan, X.; Xu, Y. Gorge Motions of Acetylcholinesterase Revealed by Microsecond Molecular Dynamics Simulations. *Sci. Rep.* **2017**, *7*, 3219.
(76) Yu, G.; Wu, W.; Zhao, Q.; Wei, X.; Lu, Q. Efficient Immobilization of Acetylcholinesterase onto Amino Functionalized Carbon Nanotubes for the Fabrication of High Sensitive Organophosphorus Pesticides Biosensors. *Biosens. Bioelectron.* **2015**, *68*, 288−294.




https://doi.org/10.1021/acs.langmuir.1c03399
*Langmuir* XXXX, XXX, XXX−XXX